
000 BIMODALITY OF SPARSE AUTOENCODER FEATURES IS 001 STILL THERE AND CAN BE FIXED 002

003 **Anonymous authors**
004

005 Paper under double-blind review
006

007 008 ABSTRACT 009

010 Sparse autoencoders (SAE) are a widely used method for decomposing LLM acti-
011 vations into a dictionary of interpretable features. We observe that this dictionary
012 often exhibits a bimodal distribution, which can be leveraged to categorize fea-
013 tures into two groups: those that are monosemantic and those that are artifacts
014 of SAE training. The cluster of noninterpretable or polysemantic features under-
015 mines the purpose of sparse autoencoders and represents a waste of potential, akin
016 to dead features. This phenomenon is prevalent across autoencoders utilizing both
017 ReLU and alternative activation functions. We propose a novel training method
018 to address this issue and demonstrate that this approach achieves improved results
019 on several benchmarks from SAE Bench. The code of the project can be found at
020 https://anonymous.4open.science/r/sae_bimodality-ICLR.
021

022 1 INTRODUCTION 023

024 1.1 THE DAWN OF SAEs AND THE FORGOTTEN PHENOMENON

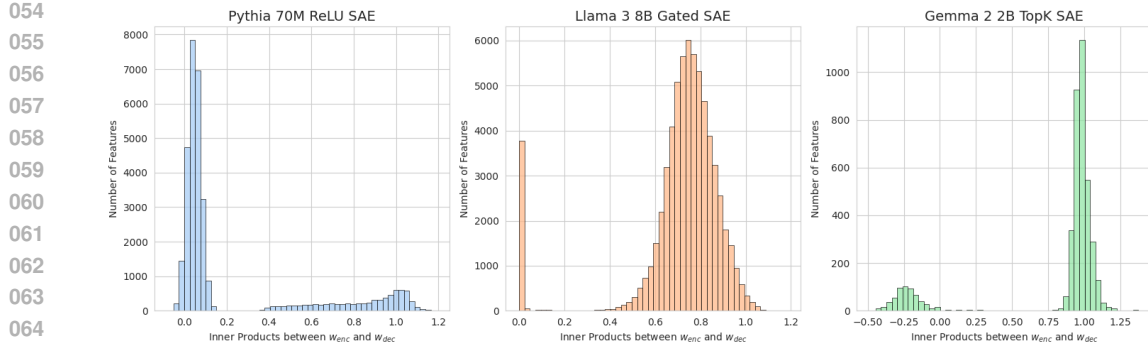
025 The superposition hypothesis (Elhage et al., 2022) posits that deep learning models represent more
026 features than they have neurons through linear directions. In (Sharkey et al., 2023), the authors
027 demonstrated that the simple architecture of sparse autoencoders (SAE) can perfectly “disentangle”
028 superposition in a synthetic dataset. In this toy model scenario, we have access which features
029 (directions in the activation space) are ground truth. The key challenge when applying SAEs to real
030 language data lies in measuring a quality of features when there is no ground truth. The proposed
031 method involves the following steps:
032

- 033 • Train a sparse autoencoder A on a dictionary of size N .
- 034 • Train another sparse autoencoder B on a dictionary of a larger size.
- 035 • Check what features are similar between the two by measuring **maximal cosine similarity**
036 **(MCS)** between feature i from A and the entire dictionary from the larger dictionary B .

037 The rationale is that features identified independently by two dictionaries are, in a sense, univer-
038 sal.” Following this procedure, for every feature i , a scalar score MCS_i is obtained, which serves
039 as a proxy for feature quality, monosemanticity, or universality. Surprisingly, it was soon observed
040 that these scores follow a clear bimodal distribution (Cunningham & Riggs, 2023). Moreover, the
041 lower values cluster closely with the distribution of randomly generated vectors (Huben, 2023). Sub-
042 sequent manual and automatic approaches to interpretability (Bills et al., 2023) confirmed that the
043 MCS value is positively correlated with feature monosemanticity. In (Riggs, 2023), the authors man-
044 ually inspected features by sorting them in descending order based on the MCS score and discovered
045 that the top-ranked features are monosemantic. Furthermore, (Cunningham, 2023) demonstrated that
046 the top-150 MCS features exhibit higher interpretability scores compared to random ones.
047

048 1.2 A SIMPLER FEATURE QUALITY PROXY 049

050 The observation that MCS scores can be used to assess the quality of SAE features and distinguish
051 between “true” directions and random artifacts appears to have been overlooked. This insight is
052 notably absent in the main culmination paper (Huben et al., 2023) and is only briefly mentioned in
053 a footnote in the independent Anthropic work (Bricken et al., 2023). We speculate that the primary



054
055
056
057
058
059
060
061
062
063
064
065
066
067
068
069
070
071
072
073
074
075
076
077
078
079
080
081
082
083
084
085
086
087
088
089
090
091
092
093
094
095
096
097
098
099
100
101
102
103
104
105
106
107
Figure 1: We can observe the bimodality of SAE features across different models and SAE architectures. The SAE details are described in B

reason for its neglect is the computational cost of the described method, as calculating MCS scores necessitates training an additional larger dictionary.

In our work, we revisit this idea by:

- Proposing a simpler scalar proxy for feature quality that does not require any data or additional training.
- Demonstrating that this score remains bimodal even in modern SAE variants, such as TopK, Gated, and JumpReLU.
- Establishing a positive correlation between the proposed score and the autointerpretability score.
- Proposing a novel training method to eliminate bimodality by design.
- Demonstrating that the proposed method outperforms standard training across multiple benchmarks, models, dictionary sizes, sparsities, and activation functions.

2 BACKGROUND ON SPARSE AUTOENCODERS

Let \mathbb{R}^n represent the activation space of a deep learning model, such as the residual stream of a large language model (LLM). The goal of a sparse autoencoder (SAE) is to decompose the activation of a data point into a sparse linear combination of features from a dictionary of size m . It has been shown (Huben et al., 2023; Bricken et al., 2023) that such features are more interpretable than neuron basis.

The encoder and decoder parts are defined as follows:

$$\mathbf{f}(\mathbf{x}) := \text{ReLU}(\mathbf{W}^{enc} \mathbf{x} + \mathbf{b}^{enc}),$$

$$\hat{\mathbf{x}} := \mathbf{W}^{dec} \mathbf{f}(\mathbf{x}) + \mathbf{b}^{dec},$$

where $\mathbf{f}(\mathbf{x}) \in \mathbb{R}^m$ is the sparse latent vector and $\hat{\mathbf{x}} \in \mathbb{R}^n$ is the reconstructed output, $\mathbf{W}^{enc} \in \mathbb{R}^{m \times n}$, $\mathbf{W}^{dec} \in \mathbb{R}^{n \times m}$ are the encoder and decoder matrices, respectively, $\mathbf{b}^{enc} \in \mathbb{R}^m$, $\mathbf{b}^{dec} \in \mathbb{R}^n$ are the encoder and decoder biases, respectively.

The loss is a weighted sum of the reconstruction L^2 loss and the L^1 penalty to enforce sparsity. That is

$$\mathcal{L} = \mathcal{L}_R + \lambda \mathcal{L}_P,$$

where

$$\mathcal{L}_R = \|\hat{\mathbf{x}} - \mathbf{x}\|^2$$

and

$$\mathcal{L}_P = \|\mathbf{f}(\mathbf{x})\|_1.$$

The scalar λ is a tunable hyperparameter that controls the sparsity of the autoencoder. An important property of these equations is their homogeneity: multiplying the encoder and dividing the decoder

108 by any scalar results in the same reconstruction. Without additional constraints, training could
109 *cheat* by making the sparsity loss \mathcal{L}_P arbitrary small. This seemingly straightforward issue requires
110 nontrivial solutions. Two methods have been proposed by researchers:
111

112 **Normalization** of the columns of the decoder matrix W^{dec} (Bricken et al., 2023; Huben et al.,
113 2023). This approach requires careful synchronization with gradient updates. In (Bricken et al.,
114 2023; Gao et al., 2025), authors project away gradient information parallel to the decoder vectors to
115 account for interactions between the Adam optimizer and normalization. In the code (Samuel Marks
116 & Mueller, 2024), authors implement a constrained version of the Adam optimizer instead.
117

118 **Reformulation** was used instead in (Conerly et al., 2024). More precisely, they change the L^1
119 norm to the weighted norm with the weights being equal to the L^2 norms of the decoder columns:
120

$$\mathcal{L}_P = \sum_i \mathbf{f}_i(\mathbf{x}) \|W_{\cdot, i}^{dec}\|_2.$$

122 This reformulation solves the homogeneity problem. Indeed, the trick with multiplication and division
123 by the same scalar does not affect the proposed \mathcal{L}_P . In line with this best practice, we also use
124 the reformulation method and do not normalize the decoder columns.
125

126 We have detailed this homogeneity problem because a deep understanding of underlying symmetries
127 is crucial for identifying better inductive biases. Indeed, in the main section of our work (5), we will
128 apply a novel reformulation method to eliminate sparse autoencoder feature bimodality.
129

130 In this paper, we primarily analyze and improve standard ReLU sparse autoencoders. However, we
131 will also mention alternative architectures, such as TopK (Gao et al., 2025), Gated (Rajamanohar-
132 an et al., 2024), and JumpReLU (Rajamanoharan et al., 2025), which employ different activation
133 functions and training procedures.
134

3 MEASURING ALIGNMENT BETWEEN ENCODER AND DECODER

3.1 ALIGNMENT SCORE - HEURISTIC MOTIVATION

138 According to the **linear representation hypothesis** (and the related **superposition hypothesis**),
139 deep learning models represent concepts as directions in the activation space. SAEs learn these
140 directions in an unsupervised manner. Indeed, each feature $i \in \{1, \dots, m\}$ corresponds to the row
141 vector $W_{i, \cdot}^{enc}$ and the column vector $W_{\cdot, i}^{dec}$. It is not clear which of them is the *true* feature vector.
142 In practice, the encoder vector is used for the concept detection and the decoder vector is used for
143 the model steering (see details in (Wu et al., 2025)). Observe that intuitively these two vectors (the
144 encoder and decoder ones) should be similar. Indeed, in (Huben et al., 2023), the authors use this
145 rationale to tie the encoder and decoder weights, that is: (see the footnote 2 there) $W^{enc} = (W^{dec})^T$.
146 In the tied weights scenario, both vectors coincide (assuming normalization). However, this is not a
147 common practice, and most modern SAEs do not adopt this procedure.
148

Based on this intuition, we propose the following measure as a proxy for feature quality:

$$a_i = W_{i, \cdot}^{enc} \cdot W_{\cdot, i}^{dec}, \quad (1)$$

151 where $i \in \{1, \dots, m\}$ and \cdot is the inner product in \mathbb{R}^n . Equivalently, these is i -th diagonal element
152 of the matrix product $W^{enc}W^{dec}$. We suspect that values of a_i which are negative or close to 0
153 correspond to not interpretable features which are the artifact of SAE training. We refer to these
154 scalars as **alignment scores**.
155

156 While the motivation for this section is based on heuristics, we also provide more precise arguments
157 for introducing this score, grounded in an analysis of toy models, in the next subsection. One of
158 the main reasons for using the inner product formulation is the homogeneity property described in
159 the previous subsection. Note that the alignment score (Equation 1) remains invariant with respect
160 to multiplication of the encoder and division of the decoder by the same scalar. We emphasize that
161 preserving this structural algebraic property is crucial in constructing the alignment score. This
exhibits stronger scale invariance with respect to both variables.
162

162 3.2 ALIGNMENT SCORE SHOULD BE CLOSE TO 1 - TOY MODEL ARGUMENT
163

164 In this subsection we will show that the alignment score is not just an ad-hoc formula and show that
165 it should be cluster close to 1. This will be confirmed empirically in the experiments.

166 Let us consider one of the simplest toy model: the activation space is two dimensional, that is $n = 2$
167 and there is only one feature in a sparse autoencoder $m = 1$. Moreover, we ignore biases and use
168 the training set of just a one single point $\mathbf{x} \in \mathbb{R}^2$. We also ignore the sparsity penalty, so the setting
169 is:

170
$$f(\mathbf{x}) = \text{ReLU}(w^{enc} \cdot \mathbf{x}),$$

171

172
$$\hat{\mathbf{x}} = f(\mathbf{x})w^{dec},$$

173

174 where w^{enc} and w^{dec} are vectors and \cdot denotes an inner product in \mathbb{R}^2 . The latent $f(\mathbf{x})$ is just a
175 scalar because we set $m = 1$.

176 Naturally, this is a very artificial setting and the autoencoder can just learn the identity. However, as
177 we will see, the ReLU nonlinearity makes the training dynamics not that trivial. Now let us check,
178 when this toy model can perfectly reconstruct the input, that is when $\hat{\mathbf{x}} = \mathbf{x}$. We have:

179
$$\mathbf{x} = \text{ReLU}(w^{enc} \cdot \mathbf{x})w^{dec}$$

180

181 Observe that \mathbf{x} and w^{dec} must be parallel, so $\mathbf{x} = \alpha w^{dec}$ for some scalar constant α . Hence we
182 obtain
183

$$\alpha w^{dec} = \text{ReLU}(\alpha w^{enc} \cdot w^{dec})w^{dec}.$$

184

185 This leads to our desired equation:

186
$$1 = w^{enc} \cdot w^{dec}.$$

187

188 In fact, this single training point example was the first “experiment” done in this research project
189 and the connection with the MCS and the bimodality phenomenon were discovered later.

190 The presented toy experiment is very crude and simplified, but as we will see, it scales effectively to
191 real sparse autoencoders. It mirrors the illustrative example from (Benjamin Wright, 2024), which
192 the authors used to explain the feature suppression/shrinkage effect.

193
194 4 PRELIMINARY EXPERIMENTS

195
196 4.1 EXPERIMENT 1: ALIGNMENT SCORES ARE BIMODAL

197 In the first experiment, we calculated the histograms of the alignment scores. The results are pre-
198 sented in Figure 1. Across different models and SAE architectures, we observed that the score
199 distribution is consistently bimodal. We suspect that this bimodality is similar to the phenomenon
200 discovered by (Huben, 2023). Additionally, a footnote in the Anthropic work (Bricken et al., 2023)
201 speculates that this same bimodality corresponds to feature frequency. It is important to empha-
202 size that, unlike MCS, the alignment score is calculated without training an additional larger SAE.
203 Furthermore, unlike feature frequency, it is derived directly from the weights without requiring ad-
204 ditional language corpus data.

205
206 4.2 EXPERIMENT 2: ALIGNMENT SCORES ARE HIGHLY CORRELATED WITH MCS

207 In the next experiment, we compared the MCS scores with the alignment scores for an autoencoder
208 trained on MLP activations from the second layer of Pythia (Biderman et al., 2023). We utilized
209 the SAE from (Riggs, 2023), where SAEs of different sizes are available. This approach avoided
210 the need to train a larger autoencoder from scratch, which would otherwise be required to calculate
211 MCS. The resulting scatter plot is shown in Figure 2. The Pearson correlation coefficient is high,
212 with a value of 0.65. Additionally, as observed, low alignment scores correspond to weaker features
213 that were not discovered by a larger interpreter model. The cluster of the best features concentrates
214 at an alignment value of 1.0 as predicted by the toy model argument from 3.2.

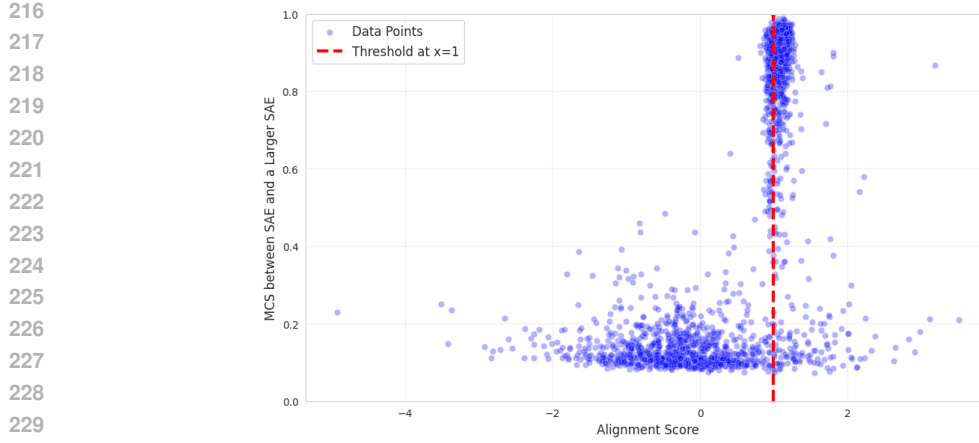


Figure 2: The scatter plot of MCS vs the alignment score. The Pearson correlation is high and equal to 0.65. The red vertical line denotes the alignment score value equal to 1.

4.3 EXPERIMENT 3: ALIGNMENT SCORES CAN BE USED TO FIND INTERPRETABLE FEATURES

In the previous experiment, we compared one proxy with another. Here, we directly assess whether alignment scores can be used to evaluate feature interpretability. We apply the commonly used autointerpretability protocol introduced in (Bills et al., 2023). In this method, LLM judge first generates a natural language description of a given neuron or direction based on a sample of maximal activations. Then, the judge model uses this generated description to score each token in another sample of texts. The interpretability score is the Pearson correlation between the LLM judge scores per token and the actual activation scores. In the case of SAEs, the activation score for feature i is equal to the encoder value $\mathbf{f}_i(\mathbf{x})$. For more details on autointerpretability protocols, see (Paulo et al., 2025).

The resulting scatter plot comparing the alignment scores with autointerpretability is presented in figure 3. The dead features for which we did not have enough non-zero activation to run the autointerpretability are presented as black dots.

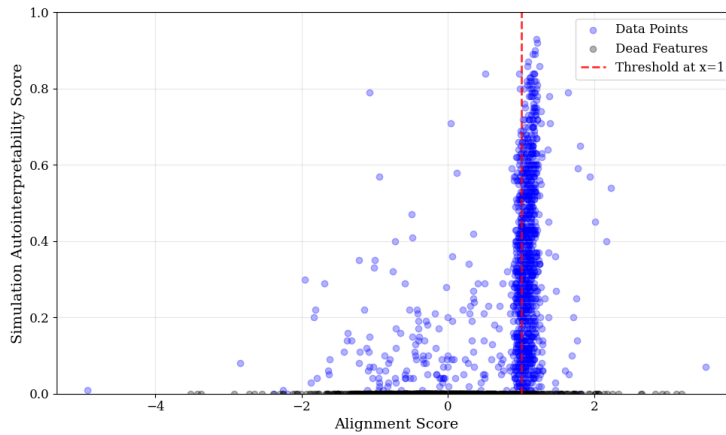


Figure 3: Autointerpretability scores vs the alignment score. The red vertical line denotes the alignment score value equal to 1. The Pearson correlation is equal to 0.32.

270 5 FIXING BIMODALITY
 271

272 From a practical standpoint, having a measure of feature quality can aid in designing more effective
 273 training algorithms for SAEs. This idea has been suggested in (Cunningham & Riggs, 2023) in
 274 the context of MCS: “*Also, the bimodal nature of the MCS scores suggests that we might be able*
 275 *to use unorthodox training strategies where we identify the convergent features and then perhaps*
 276 *freeze them while aggressively perturbing the remaining vectors*” While implementing this with
 277 the demanding MCS score was challenging, the overall simplicity of the proposed alignment score
 278 makes it feasible. Additionally, feature-aligned sparse autoencoders (Marks et al., 2024) employ a
 279 similar approach, requiring the training of two sparse autoencoders in parallel and resampling. In
 280 contrast, we propose a straightforward algebraic transformation. As discussed in 2, the encoder and
 281 decoder are defined as follows:
 282

283
$$\mathbf{f}(\mathbf{x}) := \text{ReLU}(W^{enc}\mathbf{x} + \mathbf{b}^{enc}),$$

 284
$$\hat{\mathbf{x}} := W^{dec}\mathbf{f}(\mathbf{x}) + \mathbf{b}^{dec},$$

 285

286 Now, the key idea is to leave \mathbf{b}^{enc} , \mathbf{b}^{dec} and W^{dec} as arbitrary trainable parameters and modify
 287 W^{enc} . In the proposed training method we instead of W^{enc} use a trainable parameter matrix $A \in$
 288 $\mathbb{R}^{m \times n}$ and define an encoder row $W_{i,\cdot}^{enc}$ as:
 289

290
$$W_{i,\cdot}^{enc} := A_{i,\cdot} + \alpha_i W_{\cdot,i}^{dec}, \quad (2)$$

 291 where

292
$$\alpha_i = \frac{1 - A_{i,\cdot} \cdot W_{\cdot,i}^{dec}}{\|W_{\cdot,i}^{dec}\|^2}.$$

 293

294 It is straightforward to check that:
 295

296
$$W_{i,\cdot}^{enc} \cdot W_{\cdot,i}^{dec} = 1, \quad (3)$$

 297 for every $i = 1, \dots, m$.
 298

299 Now, we just use the standard gradient descent training for parameters b^{enc} , b^{dec} , W^{dec} and A .
 300

301 In essence, we constrain the manifold of possible weights by enforcing the equation 3. Our conjecture
 302 is that this inductive bias can enhance the training of the sparse autoencoder. This approach is
 303 similar in spirit to convolutional networks. Indeed, every convolutional layer is essentially a linear
 304 layer constrained by the local receptive field (Fukushima, 1988) and weight sharing (Lecun et al.,
 305 1998). In theory, a linear layer could learn convolution during training, but incorporating this inductive
 306 bias makes the training of computer vision models more effective.

307 We will refer to the proposed method as **aligned training** and demonstrate that it outperforms standard
 308 ReLU autoencoders on several benchmarks across different sparsities, dictionary sizes, and
 309 underlying language models.

310 Moreover, because equation 3 constrains every encoder row to lie on an affine hyperplane of dimension
 311 $n - 1$, we can set the last column of A to 0 (and not train it). The resulting model can still express
 312 the same space of weights. In other words, we achieve **compression for free**; an autoencoder from
 313 aligned training has slightly fewer parameters.

314 5.1 EXPERIMENT 4: ALIGNED TRAINING ACHIEVES PARETO IMPROVEMENT ON
 315 RECONSTRUCTION METRICS
 316

317 The most basic metric used to evaluate the quality of any autoencoder is its ability to reconstruct the
 318 input. For comparing sparse autoencoders, it is essential to measure reconstruction across different
 319 sparsities, as less sparse autoencoders can trivially achieve better reconstruction (and, in the limit,
 320 even learn the identity function). The sparsity is measured by L_0 “norm”, which is the number of
 321 nonzero values in the encoded vector $\mathbf{f}(\mathbf{x})$.
 322

323 Following (Bussmann et al., 2024; Karvonen et al., 2025) we use two methods to check how good
 324 is the the autoencoder reconstruction: the explained variance and the recovered cross entropy loss
 325 (consult the Appendix A for precise formulas of these metrics).

We trained the ReLU autoencoders on the 50 million tokens from the Pile (Gao et al., 2020) using both the standard and the aligned methods and performed the test on OpenWebText. The results are presented in the figure 4. The aligned method outperforms standard training across two models, four sparsities and three dictionary sizes (see figures 16, 18 in the Appendix D.5 for 16K and 65K dictionary sizes).

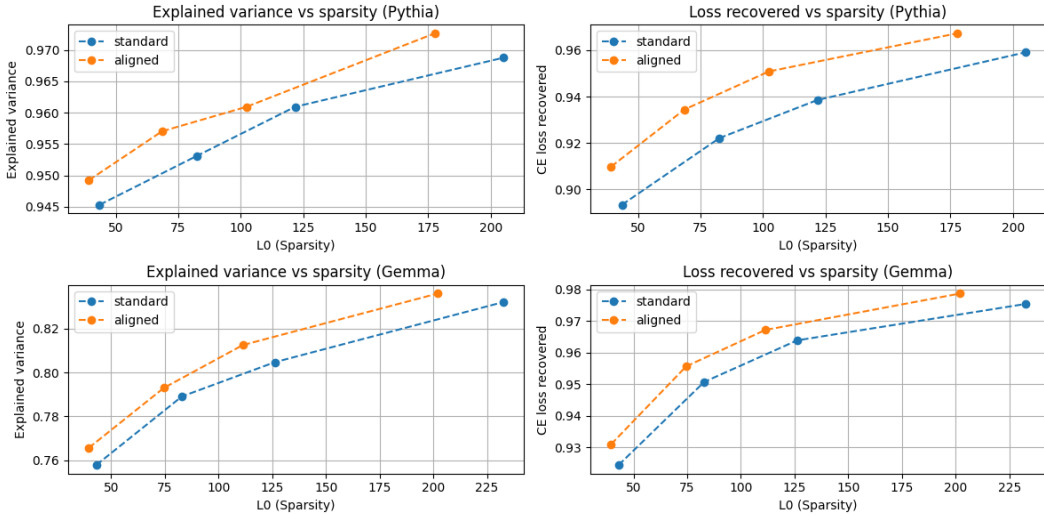


Figure 4: The proposed training methods improves the recovered cross entropy of sparse autoencoder across different sparsities. The results for the dictionary size 4096 for the 8th layer of the Pythia 160M and the 12th layer of Gemma 2 2B (Team et al., 2024)

5.2 EXPERIMENT 5: ALIGNED TRAINING AS A PARAMETER-FREE METHOD TO AVOID DEAD FEATURES

One of the notorious issues in training sparse autoencoders is the problem of dead features, where a feature does not activate for any token (Bricken et al., 2023; Gao et al., 2025; Jermyn & Templeton, 2024). This occurs because it is an easy way to minimize the sparsity loss. Several advanced measures have been developed to reduce the number of dead features:

- Resampling schemes with non-uniform probabilities (Bricken et al., 2023).
- Adding artificial gradients, known as *ghost grads*, which were introduced briefly by Anthropic (Jermyn & Templeton, 2024) but later abandoned due to their role in causing loss spikes (Adly Templeton & Henighan, 2024).
- Introducing an auxiliary loss term for dead features, as proposed in the TopK autoencoder paper (Gao et al., 2025).

We emphasize that all these methods require extensive hyperparameter tuning. In contrast, our proposed aligned training completely eliminates dead features: see Figure 5. The aligned training is parameter-free and does not require sampling or other non-differentiable operations that could destabilize training. As shown, the standard ReLU sparse autoencoder has approximately 20% dead neurons, while the aligned autoencoder has none. Furthermore, resampling and ghost grad methods focus on resurrecting dead features, whereas aligned training constrains the parameter space to prevent features from dying in the first place.

5.3 EXPERIMENT 6: SCALING TRAINING TO 500M TOKENS AND COMPARING TO STATE-OF-THE-ART

In this section, we compare aligned training to state-of-the-art ReLU sparse autoencoders provided by SAEbench. To ensure a fair comparison, we scale our training to **half a billion tokens** from The

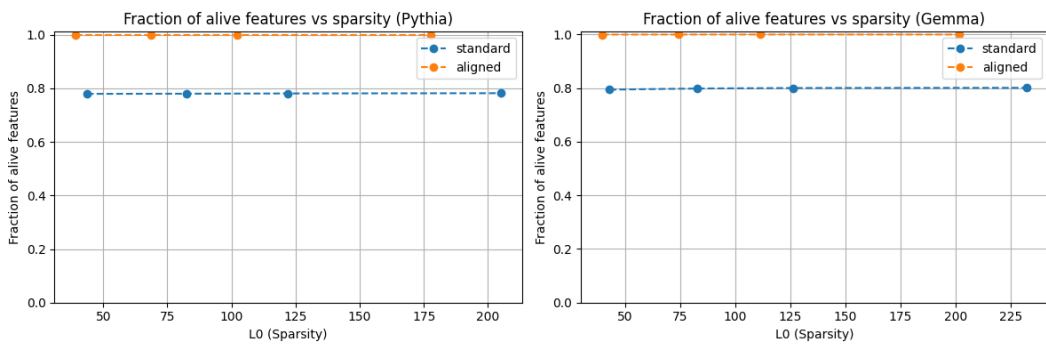


Figure 5: The proposed training method is a parameter-free approach significantly reducing the number of dead features. The results for the dictionary size 4096 for the 8th layer of the Pythia 160M and 12th layer of Gemma 2 B2.

Pile (Gao et al., 2020), matching the compute used in SAEBenchmark (recall that our formula was derived from a **1-token** toy model). As shown in Figure 6, our training surpasses both the standard SAEs trained by us and those provided by the benchmark authors. This demonstrates that the advantage is robust and not a result of cherry-picking hyperparameters. Additionally, Figure 7 shows that our training achieves a significantly lower number of dead features.

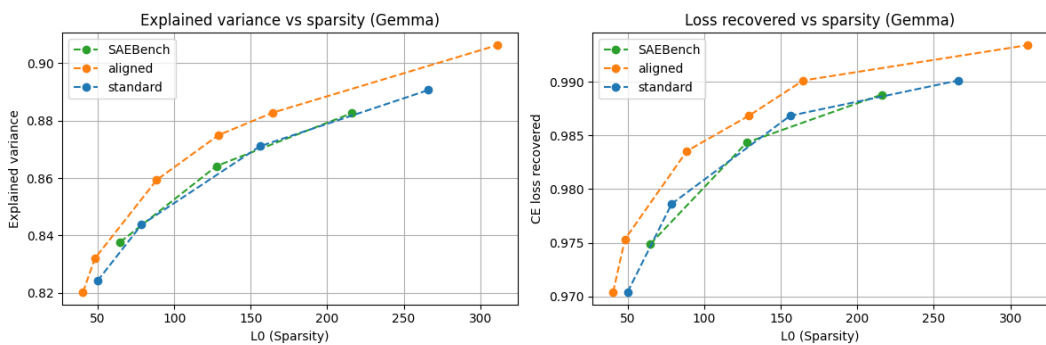


Figure 6: Reconstruction metrics comparing our method to standard (trained by us) and state-of-the-art checkpoints provided by SAE Bench. Training was conducted on half a billion tokens for layer 12 of Gemma 2 2B with a dictionary size of 65K features.

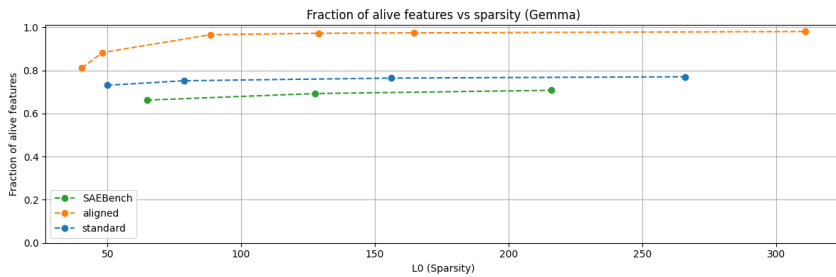
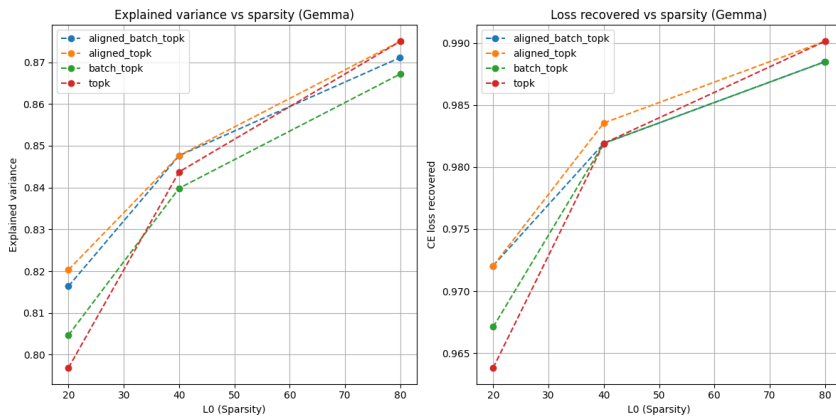
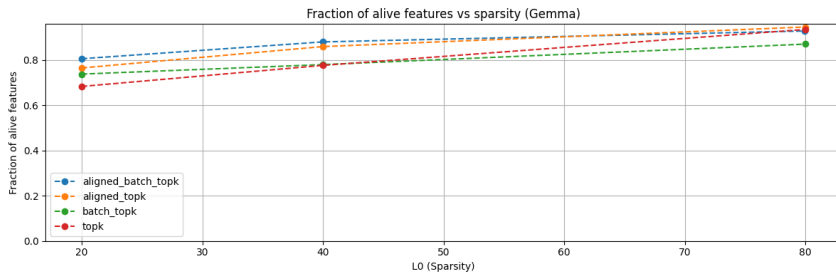


Figure 7: Fraction of alive features comparing our method to standard (trained by us) and state-of-the-art checkpoints provided by SAE Bench. Training was conducted on half a billion tokens for layer 12 of Gemma 2 2B with a dictionary size of 65K features.

432 5.4 EXPERIMENT 7: ALIGNED TRAINING IMPROVES TOPK AND BATCHTOPK
433 AUTOENCODERS
434

435 So far, we focused on standard sparse autoencoders (sometimes referred to as *vanilla* (Rajamanohar-
436 ran et al., 2025)). As shown in the first figure, bimodality also appears for different activation
437 functions. In this section we provide the results for applying the aligned training method for the
438 newer architecture of TopK sparse autoencoder (Gao et al., 2025) and its variant BatchTopK (Buss-
439 mann et al., 2024). In this approach, the sparsity is enforced not by the L^1 penalty, but by the TopK
440 activation applied on top of $f(\mathbf{x})$ (as we described in the section 2). Notice, that our training refor-
441 mulation 5 can be directly applied also in this case. While the primary motivation and toy model
442 argument were based on the ReLU model, it turns out that similar improvements can be achieved
443 even with the TopK approach.
444

445 Figure 8 presents the results of training TopK autoencoders on 50 million tokens from The Pile
446 using both the standard TopK and the aligned method. The proposed training method outperforms
447 the baseline in the low-sparsity regime, while for higher sparsities, there is no significant difference
448 between the two. Furthermore, the same pattern is observed in the number of dead neurons, as
449 shown in Figure 9.
450

463
464 Figure 8: The proposed training methods improves the TopK and BatchTopK autoencoders. The
465 results for the dictionary size 65K for the 12th layer of Gemma 2 2B.
466

477 Figure 9: The proposed training method can be applied off-the-shelf the TopK and BatchTopK
478 autoencoders, when it reduces the fraction of dead neurons. The results for the dictionary size 65K
479 for the 12th layer of Gemma 2 2B
480
481

482 REFERENCES
483

484 Jonathan Marcus Adly Templeton, Tom Conerly and Tom Henighan. Update on dictio-
485 nary learning improvements. *Transformer Circuits Thread*, 2024. URL <https://transformer-circuits.pub/2024/march-update/index.html#dl-update>.
486

486 Lee Sharkey Benjamin Wright. Addressing feature suppression in saes. *AI Alignment Forum*,
487 2024. URL <https://www.alignmentforum.org/posts/3JuSjTZYMaSeTxKk/addressing-feature-suppression-in-saes>.

488

489 Stella Biderman, Hailey Schoelkopf, Quentin Gregory Anthony, Herbie Bradley, Kyle O'Brien, Eric
490 Hallahan, Mohammad Aflah Khan, Shivanshu Purohit, USVSN Sai Prashanth, Edward Raff, et al.
491 Pythia: A suite for analyzing large language models across training and scaling. In *International
492 Conference on Machine Learning*, pp. 2397–2430. PMLR, 2023.

493

494 Steven Bills, Nick Cammarata, Dan Mossing, Henk Tillman, Leo Gao, Gabriel Goh, Ilya
495 Sutskever, Jan Leike, Jeff Wu, and William Saunders. Language models can explain neurons
496 in language models, 2023. URL <https://openaipublic.blob.core.windows.net/neuron-explainer/paper/index.html>.

497

498

499 Joseph Bloom, Curt Tigges, Anthony Duong, and David Chanin. Saelens. <https://github.com/jbloomAus/SAELens>, 2024.

500

501 Trenton Bricken, Adly Templeton, Joshua Batson, Brian Chen, Adam Jermyn, Tom Conerly, Nick
502 Turner, Cem Anil, Carson Denison, Amanda Askell, Robert Lasenby, Yifan Wu, Shauna Kravec,
503 Nicholas Schiefer, Tim Maxwell, Nicholas Joseph, Zac Hatfield-Dodds, Alex Tamkin, Karina
504 Nguyen, Brayden McLean, Josiah E Burke, Tristan Hume, Shan Carter, Tom Henighan, and
505 Christopher Olah. Towards monosemanticity: Decomposing language models with dictionary
506 learning. *Transformer Circuits Thread*, 2023. URL <https://transformer-circuits.pub/2023/monosemantic-features/index.html>.

507

508

509 Bart Bussmann, Patrick Leask, and Neel Nanda. Batchtopk sparse autoencoders. In *NeurIPS 2024
510 Workshop on Scientific Methods for Understanding Deep Learning*, 2024. URL <https://openreview.net/forum?id=d4dpOCqybL>.

511

512 Tom Conerly, Adly Templeton, Trenton Bricken, Jonathan Marcus, and Tom Henighan. Update
513 on dictionary learning improvements. *Transformer Circuits Thread*, 2024. URL
514 <https://transformer-circuits.pub/2024/april-update/index.html#training-saes>.

515

516

517 Hoagy Cunningham. Autointerpretation finds sparse coding beats alternatives. *AI Alignment Forum*,
518 2023. URL <https://www.alignmentforum.org/posts/ursraZGcpfMjCXTnn/autointerpretation-finds-sparse-coding-beats-alternatives>.

519

520

521 Hoagy Cunningham and Logan Riggs. [replication] conjecture's
522 sparse coding in small transformers. *Less Wrong*, 2023. URL
523 <https://www.lesswrong.com/posts/vBcsAw4rvLsri3JAj/replication-conjecture-s-sparse-coding-in-small-transformers>.

524

525 Maria De-Arteaga, Alexey Romanov, Hanna Wallach, Jennifer Chayes, Christian Borgs, Alexandra
526 Chouldechova, Sahin Geyik, Krishnaram Kenthapadi, and Adam Tauman Kalai. Bias in bios:
527 A case study of semantic representation bias in a high-stakes setting. In *Proceedings of the
528 Conference on Fairness, Accountability, and Transparency*, FAT* '19, pp. 120–128, New York,
529 NY, USA, 2019. Association for Computing Machinery. ISBN 9781450361255. doi: 10.1145/
530 3287560.3287572. URL <https://doi.org/10.1145/3287560.3287572>.

531

532 Nelson Elhage, Tristan Hume, Catherine Olsson, Nicholas Schiefer, Tom Henighan, Shauna Kravec,
533 Zac Hatfield-Dodds, Robert Lasenby, Dawn Drain, Carol Chen, Roger Grosse, Sam McCandlish,
534 Jared Kaplan, Dario Amodei, Martin Wattenberg, and Christopher Olah. Toy models of super-
535 position. *Transformer Circuits Thread*, 2022. URL https://transformer-circuits.pub/2022/toy_model/index.html.

536

537 Thomas Fel, Ekdeep Singh Lubana, Jacob S. Prince, Matthew Kowal, Victor Boutin, Isabel Pa-
538 padimitriou, Bin Xu Wang, Martin Wattenberg, Demba Ba, and Talia Konkle. Archetypal sae:
539 Adaptive and stable dictionary learning for concept extraction in large vision models, 2025. URL
<https://arxiv.org/abs/2502.12892>.

540 Kunihiko Fukushima. Neocognitron: A hierarchical neural network capable of visual pattern
541 recognition. *Neural Networks*, 1(2):119–130, 1988. ISSN 0893-6080. doi: [https://doi.org/10.1016/0893-6080\(88\)90014-7](https://doi.org/10.1016/0893-6080(88)90014-7). URL <https://www.sciencedirect.com/science/article/pii/0893608088900147>.

544 Leo Gao, Stella Biderman, Sid Black, Laurence Golding, Travis Hoppe, Charles Foster, Jason
545 Phang, Horace He, Anish Thite, Noa Nabeshima, Shawn Presser, and Connor Leahy. The Pile:
546 An 800gb dataset of diverse text for language modeling. *arXiv preprint arXiv:2101.00027*, 2020.
547

548 Leo Gao, Tom Dupre la Tour, Henk Tillman, Gabriel Goh, Rajan Troll, Alec Radford, Ilya Sutskever,
549 Jan Leike, and Jeffrey Wu. Scaling and evaluating sparse autoencoders. In *The Thirteenth Interna-*
550 *tional Conference on Learning Representations*, 2025. URL <https://openreview.net/forum?id=tcsZt9ZNKD>.

552 Robert Huben. [research update] sparse autoencoder features are bimodal. *From AI to ZI*, 2023. URL
553 <https://aizi.substack.com/p/research-update-sparse-autoencoder>.

554 Robert Huben, Hoagy Cunningham, Logan Riggs Smith, Aidan Ewart, and Lee Sharkey. Sparse
555 autoencoders find highly interpretable features in language models. In *The Twelfth International*
556 *Conference on Learning Representations*, 2023.

557 Adam Jermyn and Adly Templeton. Ghost grads: An improvement on resampling. *Trans-*
558 *former Circuits Thread*, 2024. URL <https://transformer-circuits.pub/2024/jan-update/index.html#dict-learning-resampling>.

561 Adam Jermyn, Adly Templeton, Joshua Batson, and Trenton Bricken. Tanh penalty in dictionary
562 learning. *Transformer Circuits Thread*, 2024. URL <https://transformer-circuits.pub/2024/feb-update/index.html#dict-learning-tanh>.

564 Adam Karvonen, Can Rager, Samuel Marks, and Neel Nanda. Evaluating sparse autoencoders on
565 targeted concept erasure tasks, 2024a. URL <https://arxiv.org/abs/2411.18895>.

567 Adam Karvonen, Benjamin Wright, Can Rager, Rico Angell, Jannik Brinkmann, Logan Riggs
568 Smith, Claudio Mayrink Verdun, David Bau, and Samuel Marks. Measuring progress in dictio-
569 nary learning for language model interpretability with board game models. In *ICML 2024 Work-*
570 *shop on Mechanistic Interpretability*, 2024b. URL <https://openreview.net/forum?id=qzsDKwGJyB>.

572 Adam Karvonen, Can Rager, Johnny Lin, Curt Tigges, Joseph Bloom, David Chanin, Yeu-Tong
573 Lau, Eoin Farrell, Callum McDougall, Kola Ayonrinde, Demian Till, Matthew Wearden, Arthur
574 Conmy, Samuel Marks, and Neel Nanda. Saebench: A comprehensive benchmark for sparse
575 autoencoders in language model interpretability, 2025. URL <https://arxiv.org/abs/2503.09532>.

577 Y. Lecun, L. Bottou, Y. Bengio, and P. Haffner. Gradient-based learning applied to document recog-
578 nition. *Proceedings of the IEEE*, 86(11):2278–2324, 1998. doi: 10.1109/5.726791.

579

580 Jannik Brinkmann Logan Riggs Smith. Improving sae's by sqrt()-ing l1 &
581 removing lowest activating features. *AI Alignment Forum*, 2024. URL
582 <https://www.alignmentforum.org/posts/YiGs8qJ8aNBgwt2YN/improving-sae-s-by-sqrt-ing-l1-and-removing-lowest>.

584 Luke Marks, Alasdair Paren, David Krueger, and Fazl Barez. Enhancing neural network inter-
585 pretability with feature-aligned sparse autoencoders, 2024. URL <https://arxiv.org/abs/2411.01220>.

587 Samuel Marks, Can Rager, Eric J Michaud, Yonatan Belinkov, David Bau, and Aaron Mueller.
588 Sparse feature circuits: Discovering and editing interpretable causal graphs in language models.
589 In *The Thirteenth International Conference on Learning Representations*, 2025. URL <https://openreview.net/forum?id=I4e82CIDxv>.

591 Gonçalo Santos Paulo, Alex Troy Mallen, Caden Juang, and Nora Belrose. Automatically interpret-
592 ing millions of features in large language models. In *Forty-second International Conference on*
593 *Machine Learning*, 2025. URL <https://openreview.net/forum?id=EemtbhJOXc>.

594 Gonçalo Paulo and Nora Belrose. Sparse autoencoders trained on the same data learn different
595 features, 2025. URL <https://arxiv.org/abs/2501.16615>.

596

597 Senthooran Rajamanoharan, Arthur Conmy, Lewis Smith, Tom Lieberum, Vikrant Varma,
598 János Kramár, Rohin Shah, and Neel Nanda. Improving sparse decomposition of lan-
599 guage model activations with gated sparse autoencoders. In A. Globerson, L. Mackey,
600 D. Belgrave, A. Fan, U. Paquet, J. Tomczak, and C. Zhang (eds.), *Advances in Neu-
601 ral Information Processing Systems*, volume 37, pp. 775–818. Curran Associates, Inc.,
602 2024. URL https://proceedings.neurips.cc/paper_files/paper/2024/file/01772a8b0420baec00c4d59fe2fbace6-Paper-Conference.pdf.

603

604 Senthooran Rajamanoharan, Tom Lieberum, Nicolas Sonnerat, Arthur Conmy, Vikrant Varma, Janos
605 Kramar, and Neel Nanda. Jumping ahead: Improving reconstruction fidelity with jumpReLU
606 sparse autoencoders, 2025. URL <https://openreview.net/forum?id=mMPaQzgZAN>.

607

608 Logan Riggs. (tentatively) found 600+ monosemantic features in a small
609 lm using sparse autoencoders. *AI Alignment Forum*, 2023. URL
610 <https://www.alignmentforum.org/posts/wqRqb7h6ZC48iDgfk/tentatively-found-600-monosemantic-features-in-a-small-lm>.

611

612 Alex Rogozhnikov. Einops: Clear and reliable tensor manipulations with einstein-like notation. In
613 *International Conference on Learning Representations*, 2022. URL <https://openreview.net/forum?id=oapKSVM2bcj>.

614

615 Adam Karvonen Samuel Marks and Aaron Mueller. *dictionary_learning*, 2024. URL https://github.com/saprmarks/dictionary_learning.

616

617 Lee Sharkey, Dan Braun, and Beren Millidge. Taking features out of su-
618 perposition with sparse autoencoders. *Alignment Forum*, 2023. URL
619 <https://www.alignmentforum.org/posts/z6QQJbtpkEAX3Aojj/interim-research-report-taking-features-out-of-superposition>.

620

621 Xiangchen Song, Aashiq Muhamed, Yujia Zheng, Lingjing Kong, Zeyu Tang, Mona T. Diab, Vir-
622 ginia Smith, and Kun Zhang. Position: Mechanistic interpretability should prioritize feature
623 consistency in saes, 2025. URL <https://arxiv.org/abs/2505.20254>.

624

625 Gemma Team, Morgane Riviere, Shreya Pathak, Pier Giuseppe Sessa, Cassidy Hardin, Surya Bhu-
626 patiraju, Léonard Hussenot, Thomas Mesnard, Bobak Shahriari, Alexandre Ramé, Johan Fer-
627 ret, Peter Liu, Pouya Tafti, Abe Friesen, Michelle Casbon, Sabela Ramos, Ravin Kumar, Char-
628 line Le Lan, Sammy Jerome, Anton Tsitsulin, Nino Vieillard, Piotr Stanczyk, Sertan Girgin,
629 Nikola Momchev, Matt Hoffman, Shantanu Thakoor, Jean-Bastien Grill, Behnam Neyshabur,
630 Olivier Bachem, Alanna Walton, Aliaksei Severyn, Alicia Parrish, Aliya Ahmad, Allen Hutchi-
631 son, Alvin Abdagic, Amanda Carl, Amy Shen, Andy Brock, Andy Coenen, Anthony Laforgue,
632 Antonia Paterson, Ben Bastian, Bilal Piot, Bo Wu, Brandon Royal, Charlie Chen, Chintu Kumar,
633 Chris Perry, Chris Welty, Christopher A. Choquette-Choo, Danila Sinopalnikov, David Wein-
634 berger, Dimple Vijaykumar, Dominika Rogozińska, Dustin Herbison, Elisa Bandy, Emma Wang,
635 Eric Noland, Erica Moreira, Evan Senter, Evgenii Eltyshhev, Francesco Visin, Gabriel Rasskin,
636 Gary Wei, Glenn Cameron, Gus Martins, Hadi Hashemi, Hanna Klimczak-Plucińska, Harleen
637 Batra, Harsh Dhand, Ivan Nardini, Jacinda Mein, Jack Zhou, James Svensson, Jeff Stanway, Jetha
638 Chan, Jin Peng Zhou, Joana Carrasqueira, Joana Iljazi, Jocelyn Becker, Joe Fernandez, Joost van
639 Amersfoort, Josh Gordon, Josh Lipschultz, Josh Newlan, Ju yeong Ji, Kareem Mohamed, Kar-
640 tikeya Badola, Kat Black, Katie Millican, Keelin McDonell, Kelvin Nguyen, Kiranbir Sodhia,
641 Kish Greene, Lars Lowe Sjoesund, Lauren Usui, Laurent Sifre, Lena Heuermann, Leticia Lago,
642 Lilly McNealus, Livio Baldini Soares, Logan Kilpatrick, Lucas Dixon, Luciano Martins, Machel
643 Reid, Manvinder Singh, Mark Iverson, Martin Görner, Mat Velloso, Mateo Wirth, Matt Davidow,
644 Matt Miller, Matthew Rahtz, Matthew Watson, Meg Risdal, Mehran Kazemi, Michael Moynihan,
645 Ming Zhang, Minsuk Kahng, Minwoo Park, Mofi Rahman, Mohit Khatwani, Natalie Dao,
646 Nenshad Bardoliwalla, Nesh Devanathan, Neta Dumai, Nilay Chauhan, Oscar Wahltinez, Pankil
647 Botarda, Parker Barnes, Paul Barham, Paul Michel, Pengchong Jin, Petko Georgiev, Phil Culli-
648 ton, Pradeep Kuppala, Ramona Comanescu, Ramona Merhej, Reena Jana, Reza Ardeshir Rokni,
649 Rishabh Agarwal, Ryan Mullins, Samaneh Saadat, Sara Mc Carthy, Sarah Cogan, Sarah Perrin,

648 Sébastien M. R. Arnold, Sebastian Krause, Shengyang Dai, Shruti Garg, Shruti Sheth, Sue Ron-
649 ström, Susan Chan, Timothy Jordan, Ting Yu, Tom Eccles, Tom Hennigan, Tomas Kociský, Tulsee
650 Doshi, Vihan Jain, Vikas Yadav, Vilobh Meshram, Vishal Dharmadhikari, Warren Barkley, Wei
651 Wei, Wenming Ye, Woohyun Han, Woosuk Kwon, Xiang Xu, Zhe Shen, Zhitao Gong, Zichuan
652 Wei, Victor Cotrutz, Phoebe Kirk, Anand Rao, Minh Giang, Ludovic Peran, Tris Warkentin, Eli
653 Collins, Joelle Barral, Zoubin Ghahramani, Raia Hadsell, D. Sculley, Jeanine Banks, Anca Dra-
654 gan, Slav Petrov, Oriol Vinyals, Jeff Dean, Demis Hassabis, Koray Kavukcuoglu, Clement Fara-
655 bet, Elena Buchatskaya, Sebastian Borgeaud, Noah Fiedel, Armand Joulin, Kathleen Kenealy,
656 Robert Dadashi, and Alek Andreev. Gemma 2: Improving open language models at a practical
657 size, 2024. URL <https://arxiv.org/abs/2408.00118>.

658 Zhengxuan Wu, Aryaman Arora, Atticus Geiger, Zheng Wang, Jing Huang, Dan Jurafsky, Christo-
659 pher D Manning, and Christopher Potts. Axbench: Steering LLMs? even simple baselines out-
660 perform sparse autoencoders. In *Forty-second International Conference on Machine Learning*,
661 2025. URL <https://openreview.net/forum?id=K2CckZjNy0>.

662

663

A FORMULAS FOR THE RECONSTRUCTION METRICS

664

665

Explained variance is defined as

666

$$1 - \frac{\frac{1}{K} \sum_{k=1}^K \|\mathbf{x}_k - \hat{\mathbf{x}}_k\|^2}{\frac{1}{K} \sum_{k=1}^K \|\mathbf{x}_k - \boldsymbol{\mu}\|^2},$$

667

where $\boldsymbol{\mu}$ is the mean activation vector:

668

669

$$\boldsymbol{\mu} = \sum_{k=1}^K \mathbf{x}_k.$$

670

671

Cross entropy loss recovered is equal to

672

673

$$\frac{H^* - H_0}{H_{orig} - H_0},$$

674

675

where H_{orig} refers to the cross-entropy loss calculated for the model’s next-token prediction task. H^* represents the cross-entropy loss obtained by replacing the model’s activation \mathbf{x} with its SAE-reconstructed version $\hat{\mathbf{x}}$ during the forward pass. Additionally, H_0 denotes the cross-entropy loss that results from zeroing out the activation \mathbf{x} .

676

677

B TECHNICAL DETAILS

678

679

In this appendix, we provide all the technical details necessary to replicate the conducted experiments. For loading pretrained SAEs, we used the sae-lens framework (Bloom et al., 2024). In histograms 1, we utilized the following SAEs:

680

681

- For Pythia: Model 70M, residual stream at layer 3. Sae-lens release: *pythia-70m-deduped-res-sm*, id: *blocks.3.hook_resid_post*.
- For LLaMA: Model 3 8B IT, residual stream at layer 25. Sae-lens release: *llama-3-8b-it-res-jh*, id: *blocks.25.hook_resid_post*.
- For Gemma: Model 2 2B, residual stream at layer 12. Sae-lens release: *sae_bench_gemma-2-2b_topk_width-2pow12_date-1109*, id: *blocks.12.hook_resid_post_trainer_0*.

682

683

For scatter plots 2 and 3 we used the ReLU autoencoders from (Riggs, 2023): https://huggingface.co/Elriggs/autoencoder_layer_2_pythia70M_5_epochs.

684

685

For autointerpretability we used the code https://github.com/HoagyC/sparse_coding which we modified to use the open source model Gemma 3 27B IT as a judge instead of the close source GPT.

686

687

For the remaining experiments, we used the same settings as in SAEBench, specifically layer 8 of Pythia 160M and layer 12 of Gemma 2 2B.

702 C CODE IMPLEMENTATION
 703

704 For training our autoencoders, we utilized the code (Samuel Marks & Mueller, 2024) and implemented the key transform 2 using the Python function described below. For the calculating the inner products per feature, we employed the einops (Rogozhnikov, 2022) library, which provides flexible Einstein notation operations on tensors.
 708

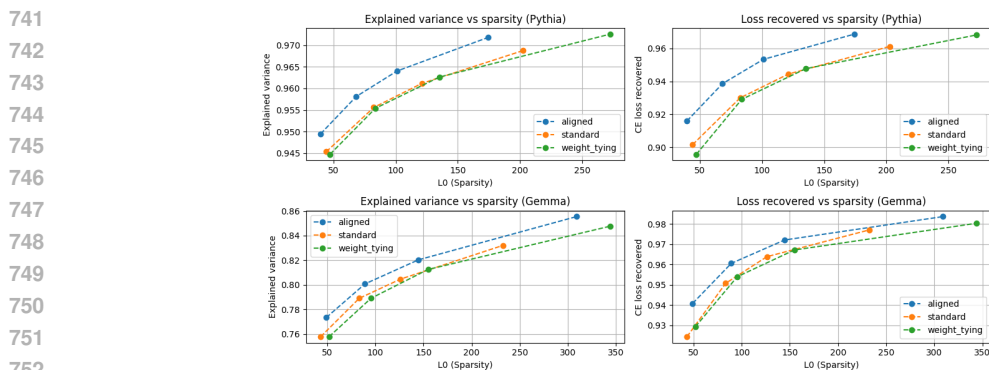
```
709 def get_the_encoder_matrix(dict_size: int,
710   ↪ encoder_weights_orthogonal_part: Float[Tensor,
711   ↪ "activation_dim-1 dict_size"], decoder_weights: Float[Tensor,
712   ↪ "dict_size activation_dim"]) -> Float[Tensor, "activation_dim
713   ↪ dict_size"]:
714   zeros = torch.zeros(1,
715   ↪ dict_size).to(encoder_weights_orthogonal_part)
716   appended = torch.concat([encoder_weights_orthogonal_part,
717   ↪ zeros])
718   inner_products = einops.einsum(decoder_weights, appended,
719   ↪ "dict_size activation_dim, activation_dim dict_size ->
720   ↪ dict_size")
721   decoder_norms_squared = decoder_weights.pow(2).sum(dim=1)
722   reparametrized = appended + decoder_weights.T * (1 -
723   ↪ inner_products) / decoder_norms_squared
724   return reparametrized
725
```

726 D ADDITIONAL EXPERIMENTS
 727

728 D.1 ALIGNMENT TRAINING IS NOT JUST WEIGHT-TYING
 729

730 As previously noted, a stronger condition can be employed to align the encoder and decoder vectors.
 731 The weight tying approach (Huben et al., 2023) assumes that the encoder and decoder vectors are
 732 identical. To evaluate these methods, we conducted experiments comparing the standard approach,
 733 weight tying, and aligned training. The results presented on 10 and 11 indicate that:
 734

- Weight tying significantly reduces the number of dead neurons but compromises reconstruction quality.
- Aligned training enhances both reconstruction performance and the proportion of active features.



753 Figure 10: Reconstruction metrics for Pythia 160M layer 8 and Gemma 2 2B layer 12 and the
 754 dictionary size of 16384 features. Weight tying underperforms.
 755

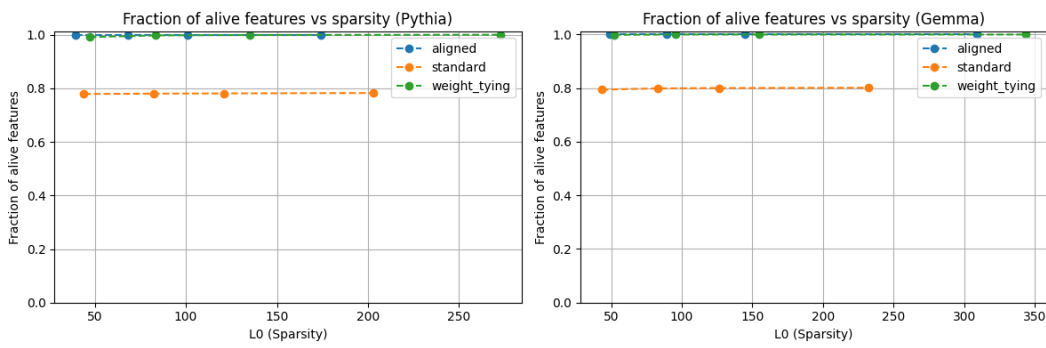


Figure 11: For Pythia 160M (layer 8) and Gemma 2B (layer 12) with a dictionary size of 16,384 features, weight tying also effectively mitigates dead features but results in suboptimal reconstruction quality.

D.2 THE ALIGNED TRAINING CAN BE COMBINED WITH P-ANNEALING

There are several non-standard methods for training ReLU autoencoders, such as square root (Logan Riggs Smith, 2024), tanh (Jermyn et al., 2024), and p-annealing (Karvonen et al., 2024b). These methods were introduced to address the issue of feature shrinkage (Benjamin Wright, 2024). Our work was motivated by a different issue—bimodality and low-quality/dead features. It is instructive to compare these approaches and explore whether they overlap or achieve synergy when applied together. As presented in the figure 12 and 13, there is indeed the improvement.

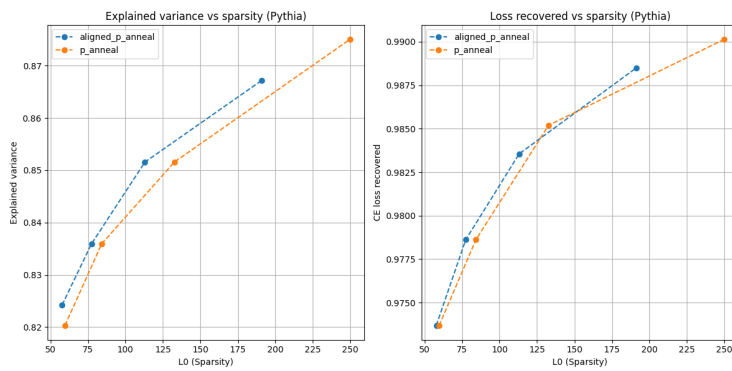


Figure 12: Reconstruction metrics for Pythia 160M layer 8 and the dictionary size of 4096 for SAE runs with 3 random seeds.

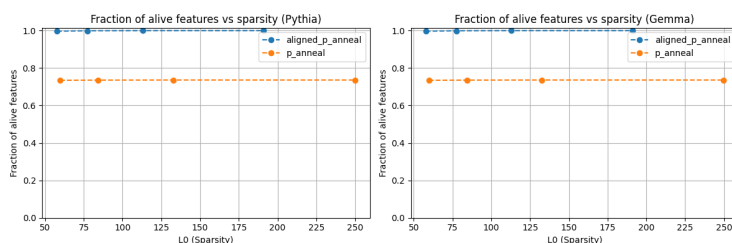
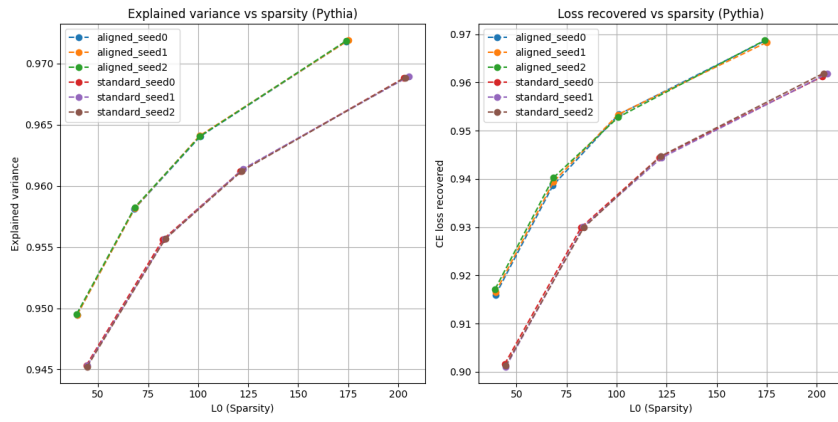


Figure 13: Fraction of alive neurons for Pythia 160M layer 8 and Gemma 2 2B layer 12 and the dictionary size of 16384 features.

810 D.3 THE RESULTS ARE ROBUST WITH RESPECT TO DIFFERENT SEEDS 811

812 In this section we perform the important validation. There is an inherent stochasticity in training
813 sparse autoencoders, hence it is crucial to check how the results change with varying random seeds.
814 As demonstrated on the figure 14 the difference is negligible.

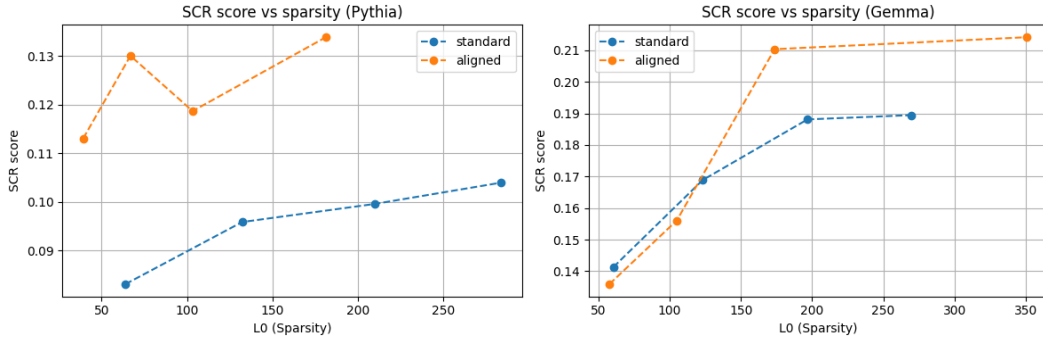


830
831 Figure 14: Reconstruction metrics for Pythia 160M layer 8 and the dictionary size of 4096 for SAE
832 runs with 3 random seeds.

833 834 835 D.4 ALIGNED TRAINING OUTPERFORMS STANDARD AUTOENCODER IN SPURIOUS 836 CORRELATION REMOVAL 837

838 The metrics used in the two previous experiments are still theoretical proxies for evaluating the
839 usefulness of an autoencoder. We also tested our proposed method on a practical downstream task
840 and found that it achieves better results. The application of sparse autoencoders to remove spurious
841 correlations was introduced in the SHIFT method (Marks et al., 2025) in the context of gender bias
842 (De-Arteaga et al., 2019) and extended in (Karvonen et al., 2024a). We used the implementation of
843 this metric from the SAEbench suite (Karvonen et al., 2025).

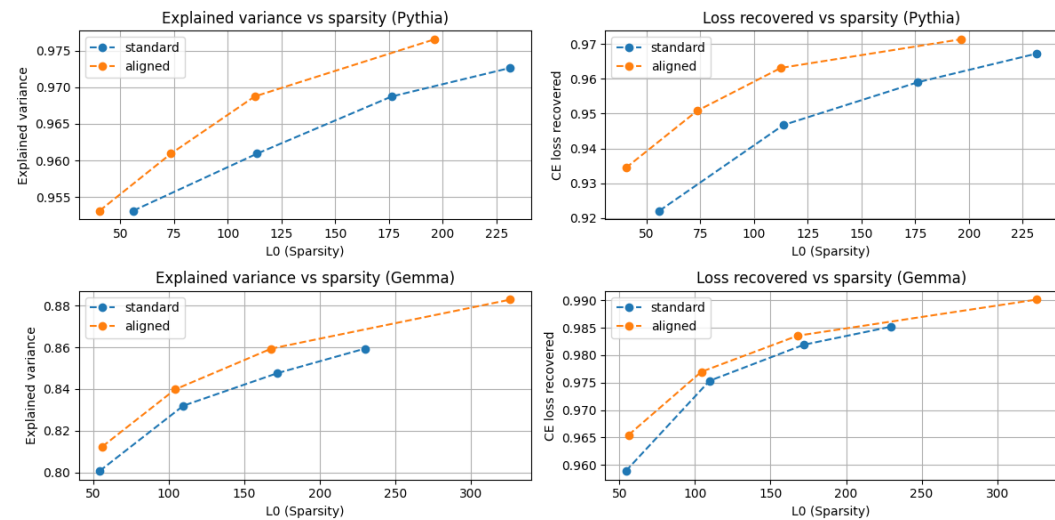
844 As shown in Figure 15, aligned training outperforms the standard method on the Pythia model. For
845 Gemma, the two methods are comparable for smaller sparsity ranges, but our method shows a clear
846 advantage for larger L_0 values.



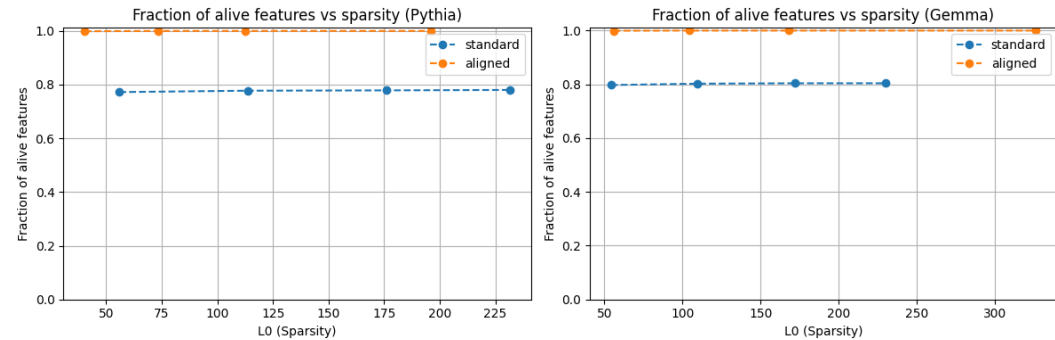
861
862 Figure 15: Results for spurious correlation removal metric from SAEbench on the dictionary size =
863 65K for Pythia 160M and Gemma 2 2B.

864 D.5 RESULTS ARE CONSISTENT FOR DIFFERENT DICTIONARY SIZES

866 In this subsection we show the reconstruction loss and dead neurons metrics for the different dictionary sizes. For 16K features consult the Figures 16 and 17. We also conducted the experiments for 867 the large dictionary of 65K, see the Figures 18 and 19.



888 Figure 16: Reconstruction metrics for Pythia 160M layer 8 and Gemma 2 2B layer 12 and the
889 dictionary size of 16384 features.



904 Figure 17: Fraction of alive neurons for Pythia 160M layer 8 and Gemma 2 2B layer 12 and the
905 dictionary size of 16384 features.

907 E CONNECTION WITH THE FEATURE CONSISTENCY

910 There is growing interest in measuring the feature consistency of sparse autoencoders, as seen in
911 recent works (Paulo & Belrose, 2025; Song et al., 2025). This issue is closely related to the MCS
912 metric we discussed, as it evaluates the similarity between SAEs with the same dictionary sizes
913 trained on different seeds.

914 Archetypical SAEs Fel et al. (2025) address this phenomenon by training models to fit the convex
915 hull of the data points, improving feature consistency. However, this approach comes at the cost of
916 degrading reconstruction metrics. This trade-off highlights a key distinction between their solution
917 and ours: aligned training improves reconstruction metrics and also reduces the fraction of dead
neurons.

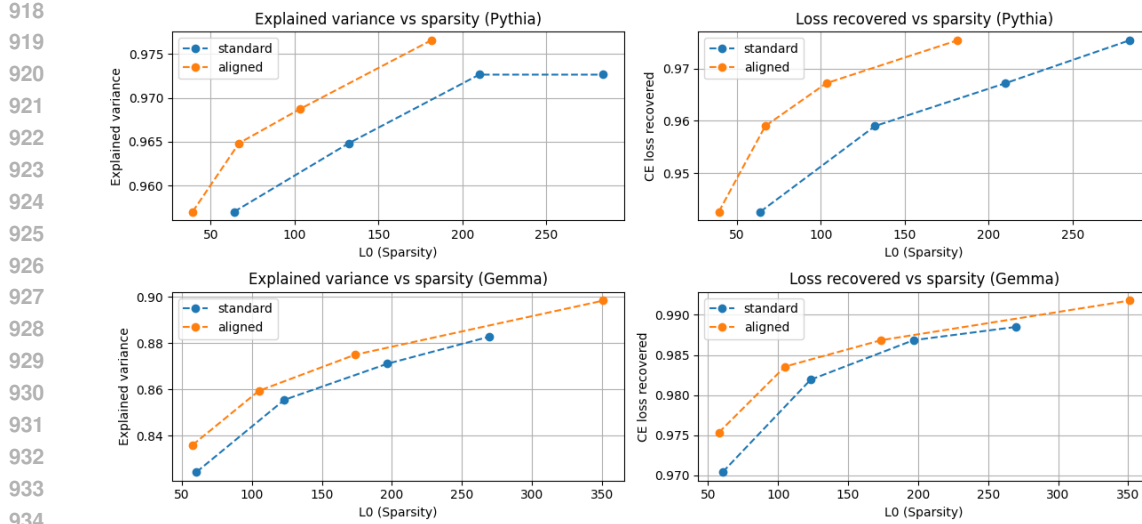


Figure 18: Reconstruction metrics for Pythia 160M layer 8 and Gemma 2 2B layer 12 and the dictionary size of 65K features.

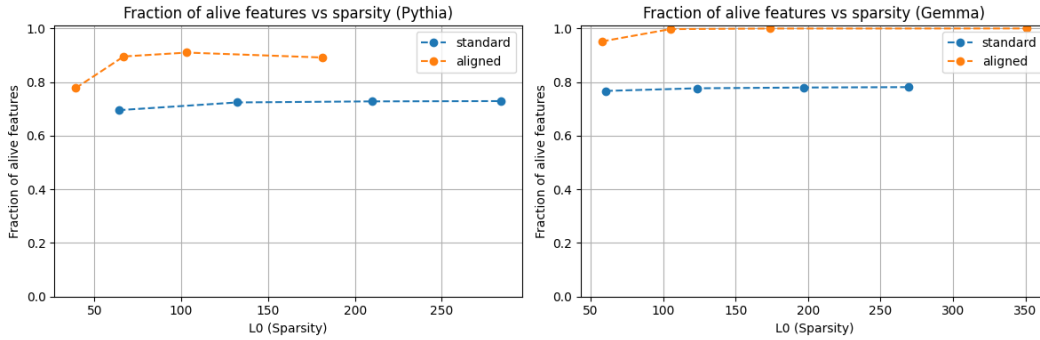


Figure 19: Fraction of alive neurons for Pythia 160M layer 8 and Gemma 2 2B layer 12 and the dictionary size of 65K features.

In follow-up experiments, we plan to evaluate how our method performs against archetypical SAEs on their proposed stability metric.

F THE BIMODALITY DYNAMICS

In this experiment, we loaded the SAEbench checkpoints from different training steps and produced the histograms of the alignment score across time, see Figure 20.

G SANITY CHECK

We also have performed a trivial sanity check that for the alignment score is indeed 1 for our training method, see the Figure 21.

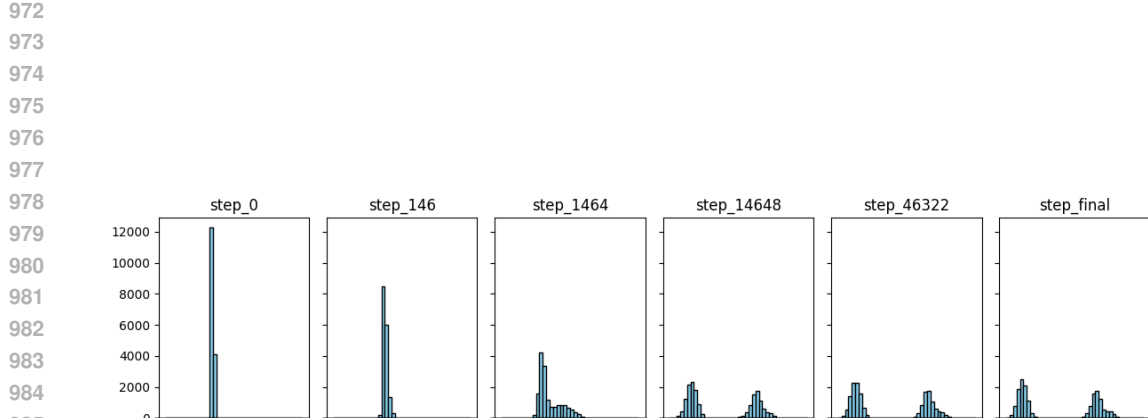


Figure 20: Creation of the bimodality during training of a TopK SAE trained on the layer 12 of Gemma 2 2B. We used checkpoints provided in SAEBench(Karvonen et al., 2025). We hypothesize that this is caused by two competing forces: useful features are pushed to the cluster with the alignment close to 1. On the other hand, useless features are pushed to the left, where they rarely activate. The second effect is caused by the sparsity goal.

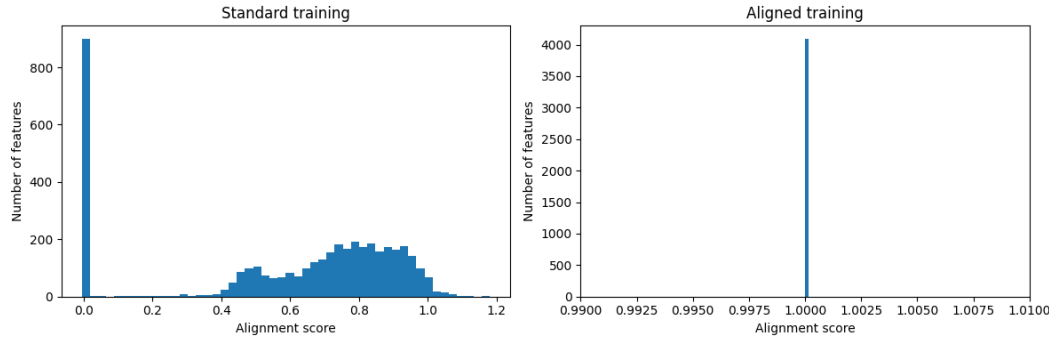


Figure 21: Histograms of alignment scores of the standard and aligned trained sparse autoencoders. The plot on the right serves as a sanity check: the proposed reformulation achieves its intended goal by forcing all alignment scores to be equal to 1, effectively preventing the creation of bimodality.